

Nonlinear Néel Spin-Orbit Torque in Centrosymmetric Antiferromagnets

Jin Cao,^{1,*} Weikang Wu,^{2,*} Huiying Liu,^{3,†} Shen Lai,¹ Cong Xiao,^{4,‡} X. C. Xie,^{4,5} and Shengyuan A. Yang⁶

¹*Institute of Applied Physics and Materials Engineering,
Faculty of Science and Technology, University of Macau, Macau, China*

²*Key Laboratory for Liquid-Solid Structural Evolution and Processing of Materials,
Ministry of Education, Shandong University, Jinan 250061, China*

³*School of Physics, Beihang University, Beijing 100191, China*

⁴*Interdisciplinary Center for Theoretical Physics and Information
Sciences (ICTPIS), Fudan University, Shanghai 200433, China*

⁵*International Center for Quantum Materials, School of Physics, Peking University, Beijing 100871, China*

⁶*Research Laboratory for Quantum Materials, Department of Applied Physics,
The Hong Kong Polytechnic University, Hong Kong, China*

Electric control of Néel vector is a central task of antiferromagnetic (AFM) spintronics. The major scheme so far relies on the linear Néel torque, which however is restricted to AFMs with broken inversion symmetry. Here, we propose a nonlinear Néel spin-orbit torque, uniquely enabling electric control in the vast class of centrosymmetric AFMs, where the existing scheme fails. Importantly, its intrinsic component, rooted in sublattice-resolved band quantum geometry, offers two additional advantages: It operates also in \mathcal{PT} -symmetric AFM insulators, where linear torque is forbidden; and it has anti-damping character, making it more efficient in driving magnetic dynamics. Combined with first-principles calculations, we predict large effect in MnRh and MnBi₂Te₄, which can be readily detected in experiment. Our work unveils a new fundamental effect, offers a new strategy of electric control in AFM systems beyond the existing paradigm, and opens the door to the field of nonlinear AFM spintronics.

The potential of antiferromagnets (AFM) in spintronics applications has received tremendous interest, due to their unique advantages, such as robustness against magnetic field perturbations, absence of stray fields, and ultrafast spin dynamics [1–3]. To make scalable devices, a central task of AFM spintronics is to realize the electric control of Néel order [4]. Currently, the main approach is via the so-called Néel torque [5–7], exerted by electrically induced local spin polarization that is *staggered* on opposite AFM spin sublattices, as illustrated in Fig. 1(a). The Néel torque and its effect on Néel vector dynamics have been successfully demonstrated in several AFMs, including CuMnAs [8–10] and Mn₂Au [11, 12], with a greatly improved operation speed up to GHz [13] or even THz scale [14].

Despite significant progress, the current scheme of Néel torque relies on linear effects and is restricted to AFMs with broken inversion symmetry \mathcal{P} [7]. Indeed, in a centrosymmetric AFM, the \mathcal{P} -invariance of magnetic moment necessitates that each magnetic sublattice also preserves \mathcal{P} . Consequently, the linearly induced spin polarization $\delta s \propto E$, being odd under \mathcal{P} , must have a zero net value on each sublattice, resulting in a vanishing Néel torque. Given that centrosymmetric AFMs constitute a very large class of AFM materials with rich functionalities, how to achieve Néel torque in these systems has become a critical challenge for AFM spintronics [1–3, 7].

In this work, we address this challenge by proposing a *nonlinear* Néel torque, driven by sublattice-staggered spin polarization nonlinearly generated by electric field [Fig. 1(b)]. This is a general effect working for both noncentrosymmetric and centrosymmetric AFMs. From

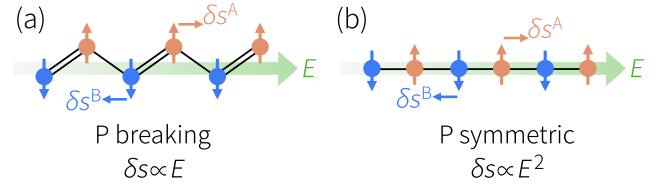


FIG. 1. Schematics of (a) linear Néel torque due to linearly field-induced staggered spin polarization in AFMs with broken inversion symmetry; and (b) nonlinear Néel torque that can operate in centrosymmetric AFMs, where the linear Néel torque is forbidden.

symmetry analysis, we show that for centrosymmetric AFMs, it is the leading order mechanism for Néel torque; and for certain noncentrosymmetric AFMs, e.g., \mathcal{PT} -symmetric AFM insulators, it also gives the dominant contribution and is of entirely intrinsic nature. Moreover, the intrinsic part of nonlinear Néel torque has anti-damping character, making it highly efficient in driving magnetic reorientations. We develop a microscopic theory for the intrinsic nonlinear Néel torque and reveal its origin in sublattice-resolved band geometry. Combining with first-principles calculations, we evaluate the proposed effect in MnRh, 3D bulk MnBi₂Te₄, and 2D even-layered MnBi₂Te₄, finding significant results that can be experimentally detected. Our work not only reveals a fundamental phenomenon in nonlinear spintronics, but also opens a new route to electrical manipulation of AFM order in a wide range of previously inaccessible systems, paving the way towards nonlinear AFM spintronics

Symmetry consideration. Consider fully compensated collinear AFM systems with two magnetic sublattices, labeled by $i = A, B$. The nonlinear spin polarization generated by applied E field on sublattice i can be expressed as

$$\delta s_a^i = \alpha_{abc}^i E_b E_c \quad (1)$$

where α_{abc}^i is the sublattice-resolved nonlinear response tensor, and the summation over repeated Cartesian indices (the subscripts here) is implied henceforth. One immediately observes that distinct from linear Néel torque, due to the additional E factor, δs^i here is even under \mathcal{P} , making the nonlinear response compatible with centrosymmetric AFMs.

The specific form of α tensor are constrained by symmetry group of AFMs. To analyze sublattice-resolved responses, we make the following decomposition of a given magnetic point group \mathcal{G} :

$$\mathcal{G} = \mathcal{G}_s + a\mathcal{G}_s, \quad (2)$$

where \mathcal{G}_s is the subgroup of operations that preserve each sublattice, and $a\mathcal{G}_s$ are the operations that switch the two sublattices, with a being any representative of this set. Moreover, in studying magnetic systems, it is important to distinguish the character of a response under time reversal operation \mathcal{T} , i.e., whether the response changes sign under the reversal of all magnetic moments. Any response tensor can be decomposed into \mathcal{T} -odd and \mathcal{T} -even parts. For a \mathcal{T} -odd response α_{abc}^i , it is constrained by

$$\begin{cases} \alpha_{a'b'c'}^i = \eta |\mathcal{O}| \mathcal{O}_{a'a} \mathcal{O}_{b'b} \mathcal{O}_{c'c} \alpha_{abc}^i, & \text{if } \mathcal{O} \in \mathcal{G}_s \\ \alpha_{a'b'c'}^i = \eta |\mathcal{O}| \mathcal{O}_{a'a} \mathcal{O}_{b'b} \mathcal{O}_{c'c} \alpha_{abc}^B, & \text{if } \mathcal{O} \in a\mathcal{G}_s \end{cases}, \quad (3)$$

where $|\mathcal{O}| = \pm 1$ is the determinant of \mathcal{O} , $\eta = -1$ for primed operations, i.e., operations involving \mathcal{T} operator, and $\eta = 1$ for nonprimed operations. The constraint (3) also applies to \mathcal{T} -even α_{abc}^i response, for which $\eta = 1$ for both primed and nonprimed operations.

To support a Néel torque, we must have: (i) \mathcal{G}_s allows components of δs^i perpendicular to the sublattice magnetization \mathbf{M}^i ; and (ii) $a\mathcal{G}_s$ allows staggered spin polarization on the two sublattices, i.e., $\delta s^A = -\delta s^B$. Based on Eq. (3), we examine the constraints from all magnetic symmetry elements on α_{abc}^i , and the results are presented in Supplemental Material [15].

Here, we highlight some important consequences from this analysis. First, many previous studies were focusing on AFMs with \mathcal{PT} or $\mathcal{T}t_{1/2}$ symmetry ($t_{1/2}$ is a half lattice translation). We note that under \mathcal{PT} , the linear Néel torque must be a \mathcal{T} -even response, however, the nonlinear torque is a \mathcal{T} -odd response. This is a crucial difference, as it determines the different character of the torque: The \mathcal{T} -odd response may correspond to an antidamping-like torque, whereas the \mathcal{T} -even response tends to give

TABLE I. Comparison of linear and nonlinear Néel torques in several commonly encountered AFM systems. Here, BCP indicates the nonlinear torque in insulating AFMs is entirely from the intrinsic BCP mechanism.

| | Linear | | Nonlinear | |
|----------------------|---------------------|--------------------|---------------------|--------------------|
| | \mathcal{T} -even | \mathcal{T} -odd | \mathcal{T} -even | \mathcal{T} -odd |
| \mathcal{P} | × | × | ✓ | ✓ |
| \mathcal{PT} | ✓ | × | × | ✓ |
| $\mathcal{T}t_{1/2}$ | × | ✓ | × | ✓ |
| Insulators | × | ✓ | × | ✓ (BCP) |

a field-like torque, and the two act on magnetic dynamics in qualitatively different ways [4]. Meanwhile, we also note that for AFM with $\mathcal{T}t_{1/2}$ symmetry, linear and nonlinear Néel torques are both of \mathcal{T} -odd character. These results are presented in Table I.

Second, there exist a number of AFMs, e.g., $L1_0$ -type manganese alloys, NiO, and 3D MnBi_2Te_4 , which possess both \mathcal{PT} and $\mathcal{T}t_{1/2}$ symmetries (This implies \mathcal{P} is also preserved). According to Table I, in such systems, linear Néel torque as well as \mathcal{T} -even nonlinear Néel torque are all prohibited, and the dominating torque is from the \mathcal{T} -odd nonlinear mechanism.

Third, the nonlinear Néel torque may also play a leading role in certain noncentrosymmetric AFMs. For example, in \mathcal{PT} -symmetric AFM *insulators* (regardless of whether \mathcal{P} is respected or not), linear Néel torque is always suppressed, because it is \mathcal{T} -even and of extrinsic origin (i.e., arising from scattering effects), which requires the presence of Fermi surface [5, 6]. Consequently, the nonlinear response also dominates such cases, and it is of entirely intrinsic nature, determined by the intrinsic quantum geometry of valence electrons (see below), rendering a new way to manipulate \mathcal{PT} -symmetric AFM insulators.

Intrinsic mechanism. We shall focus on intrinsic nonlinear Néel torque, based on the following considerations. First, this intrinsic nonlinear torque is \mathcal{T} -odd, so it is relevant to all the important cases in Table I. Particularly, for most collinear AFM insulators (with \mathcal{P} or \mathcal{PT} symmetry), it is the *only* contribution present. Second, the intrinsic nonlinear Néel torque is determined solely by the band structure, manifesting the inherent property of each material. Hence, it can be quantitatively evaluated and provides a benchmark for comparison between theory and experiment.

Based on the extended semiclassical theory [16–19], the intrinsic nonlinear electrically-induced spin polarization has been derived in ferromagnetic systems [20]. To deal with Néel torques in AFMs, we need to distinguish the two magnetic sublattices and formulate the sublattice-resolved response tensor α_{abc}^i (details in [15]). The fol-

lowing formula is obtained (we set $e = \hbar = 1$):

$$\alpha_{abc}^i = -\frac{1}{2} \int [d\mathbf{k}] f_0' (s_a^i G_{bc} + v_b \mathfrak{G}_{ac}^i + v_c \mathfrak{G}_{ab}^i) - \frac{1}{2} \int [d\mathbf{k}] f_0 \partial_{h_a^i} G_{bc} \Big|_{h^i=0}, \quad (4)$$

where we have explicitly symmetrized the two subscripts b and c , $[d\mathbf{k}]$ is a shorthand for $\sum_n dk^D / (2\pi)^D$ with D the spatial dimension of the system, the band index label n and the k dependence of quantities in the integrand are not written out explicitly for simple notations. f_0 is the Fermi-Dirac distribution, $s_a^i = \langle u_{n\mathbf{k}} | \hat{s}_a^i | u_{n\mathbf{k}} \rangle$ is the sublattice-resolved spin polarization for Bloch state $|u_{n\mathbf{k}}\rangle$, with $\hat{s}_a^i = \frac{1}{2}(\hat{s}_a \hat{P}_i + \hat{P}_i \hat{s}_a)$ and \hat{P}_i the projection operator for sublattice i , and v_a is the group velocity. h_a^i is an auxiliary field coupled to sublattice spins through a term $-s_a^i h_a^i$ [18] added to the Hamiltonian and it is taken to be zero at the end of calculation (the explicit expression of $\partial_{h_a^i} G$ is presented in [15]). There are two important band geometric quantities appearing in Eq. (4). G_{ab} , known as the momentum-space Berry-connection polarizability (BCP) [21], can be expressed in terms of interband velocity matrix element $(v_a)^{nn'}$ and band energy ε_n :

$$G_{ab} = 2\text{Re} \sum_{n' \neq n} \frac{(v_a)^{nn'} (v_b)^{n'n}}{(\varepsilon_n - \varepsilon_{n'})^3}. \quad (5)$$

Meanwhile, \mathfrak{G}_{ab}^i is the sublattice-resolved h -space BCP:

$$\mathfrak{G}_{ab}^i = -2\text{Re} \sum_{n' \neq n} \frac{(s_a^i)^{nn'} (v_b)^{n'n}}{(\varepsilon_n - \varepsilon_{n'})^3}. \quad (6)$$

We have a few remarks on this result. First, one observes that the intrinsic response contains both a Fermi surface contribution (the first line of Eq. (4)) and a Fermi sea contribution (the second line). The Fermi surface term is present only for metallic AFMs, while the Fermi sea term can operate also in insulating AFMs. Second, one can verify that the result of (4) is even under \mathcal{P} (and odd under \mathcal{T}), confirming its compatibility with centrosymmetric AFMs. It should be noted that although Eq. (4) gives the nonlinear electric spin generation on the two sublattices, to obtain the Néel torque, one needs to extract its staggered component, i.e., the antisymmetric part with $\alpha^A = -\alpha^B$. Notably, for AFMs with suitable symmetries, e.g., \mathcal{PT} or $\mathcal{T}t_{1/2}$ symmetry, α given by Eq. (4) is constrained to be staggered on the sublattices hence directly gives the Néel torque. Third, the BCPs are typically pronounced near band (anti)crossing regions in a band structure. This offers a useful guidance to enhance the nonlinear Néel torque.

As mentioned, our proposed nonlinear effect could be the dominant source of Néel torque for a large class of AFM materials. Below, we apply our theory to three

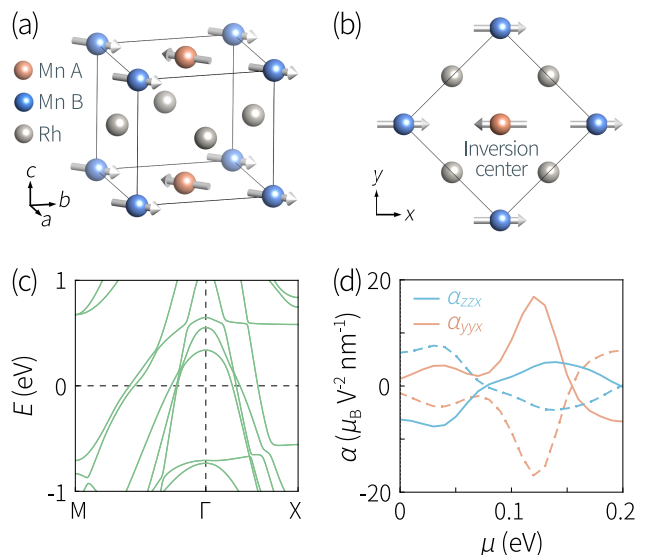


FIG. 2. (a) Structure of $L1_0$ -type AFM MnRh. (b) Top view of (a). (c) Calculated band structure of MnRh. (d) Calculated α_{yyx}^i and α_{zzx}^i near the Fermi level. Solid (dashed) lines correspond to $i = A$ (B). $T = 100$ K is taken in the calculation of (d).

representative examples, including the centrosymmetric AFMs MnRh and bulk MnBi_2Te_4 , and \mathcal{PT} -symmetric even-layer MnBi_2Te_4 .

Application to MnRh. Manganese alloys form a large family of magnetic materials [22]. Most of them are AFM with high Néel temperature and possess inversion symmetry. Here, we consider $L1_0$ -type MnRh, which has a tetragonal structure with D_{4h} point group (Fig. 2(a)). In its AFM ground state, the Néel vector is in-plane and along the $[110]$ direction [23–25]. Our first-principles calculations (details in [15]) find the magnetic moment at Mn site is $\sim 3.1 \mu_B$, consistent with previous study [25].

The magnetic point group of MnRh is $mmm1'$, preserving both \mathcal{P} and \mathcal{PT} (hence also $\mathcal{T}t_{1/2}$) symmetries. According to Table I, the linear response is forbidden, and the Néel torque is dominated by \mathcal{T} -odd nonlinear response which is enforced to be sublattice-staggered. In the coordinate system of Fig. 2(b), our symmetry analysis shows that Néel torque is associated with two independent response coefficients α_{yyx}^i and α_{zzx}^i .

Figure 2(c) shows the calculated band structure of MnRh, which is an AFM metal. The intrinsic α_{yyx}^i and α_{zzx}^i determined by the band structure are computed and plotted versus chemical potential in Fig. 2(d). As mentioned, the Néel vector of this system tends to be in-plane: the in-plane magnetic anisotropy energy (MAE) \sim a few μeV is much smaller than the out-of-plane MAE ~ 0.1 meV [24, 25]. Hence, it should be easier to rotate the Néel vector in xy -plane. Consider α_{zzx}^i , which takes a value of $6 \mu_B \text{V}^{-2} \text{nm}^{-1}$ at intrinsic Fermi level. Under a typical current density of 10^8 A/cm² [14, 26] applied

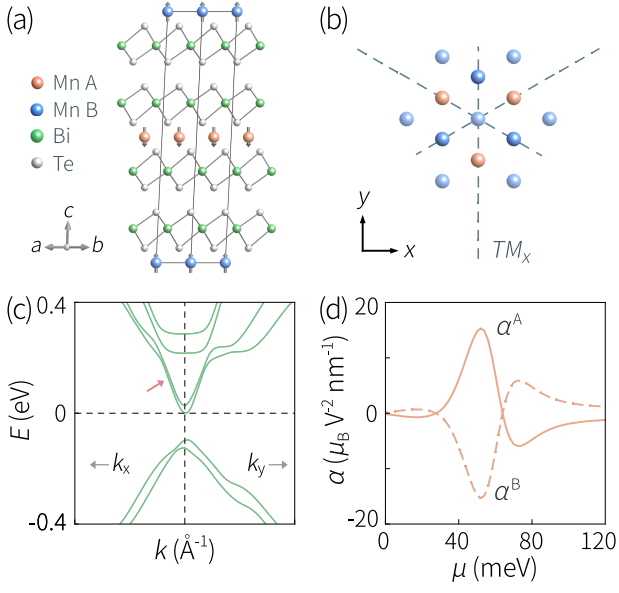


FIG. 3. (a) Structure of AFM bulk MnBi_2Te_4 . (b) Top view of the two Mn sublattices. Other atoms are not shown. (c) Calculated band structure of bulk MnBi_2Te_4 . (d) Calculated α_{yyy}^A and α_{yyy}^B versus μ on the electron doping side. $T = 20$ K is taken in the calculation of (d).

in the xz -plane (corresponding to an E field $\sim 10^6$ V/m, using the reported resistivity of $100 \mu\Omega \text{ cm}$ [27]), we find that the nonlinearly generated staggered spin density can reach a large value $\sim 0.6 \times 10^{-5} \mu_B/\text{nm}^3$. The generated Néel torque is

$$\mathbf{T}^i = \mathbf{M}^i \times \mathbf{B}_T^i, \quad (7)$$

where \mathbf{M}^i is the magnetization on sublattice i , and

$$\mathbf{B}_T^i \approx - (J_{\text{sd}}/\mu_B) \delta \mathbf{s}^i / M^i \quad (8)$$

is the effective spin-orbit magnetic field from $\delta \mathbf{s}^i$, where J_{sd} is the exchange coupling strength between carrier spin and background magnetization. It is noted that the \mathcal{T} -odd nonlinear torque here is *antidamping-like*. Such a torque is more efficient than field-like torque in driving magnetic reorientation, as it competes with anisotropic barrier multiplied by the Gilbert damping α_G , whose strength is relatively small [4]. To capture this character, one usually looks at the effective strength B_T/α_G . Taking typical values $J_{\text{sd}} \sim 1$ eV and $\alpha_G \sim 0.01$ [5, 28], we find $B_T^i/\alpha_G \sim 180$ mT (corresponding to an energy scale $\sim 30 \mu\text{eV}$), which is a significant value compared to in-plane MAE and should be able to drive magnetic reorientation in MnRh.

Application to doped 3D MnBi_2Te_4 . Next, we consider the 3D bulk MnBi_2Te_4 . It is an van der Waals layered AFM material, which have been attracting great interest in recent years [29–42]. As illustrated in Fig. 3(a), MnBi_2Te_4 consists of Te-Bi-Te-Mn-Te-Bi-Te septuple

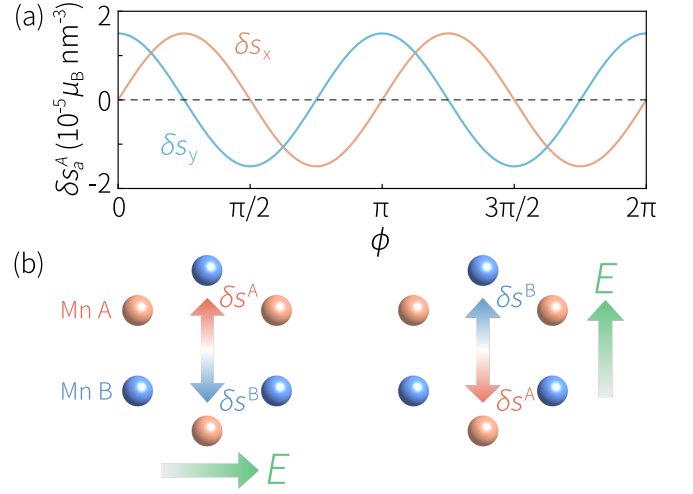


FIG. 4. (a) Angular dependence of the nonlinearly generated staggered spin density in bulk MnBi_2Te_4 . (b) Schematic figure showing the flip of nonlinear Néel torque when the driving field is rotated by $\pi/2$.

layers stacked along the c axis (z direction). The AFM ordering is of A type, i.e., in each septuple layer, the Mn spins are ferromagnetically coupled, with an easy axis along z , whereas neighboring layers are coupled in AFM manner.

The AFM state has magnetic point group $-3m1'$. It preserves \mathcal{P} , so linear Néel torque is not allowed. In addition, \mathcal{PT} and $\mathcal{T}t_{1/2}$ also exist, so \mathcal{T} -odd nonlinear response makes the dominant Néel torque. Constrained by $\mathcal{G}_s = -3m'$, for driving field in the xy -plane, we find that there is only one independent response tensor component, with $\alpha_{xxy}^i = \alpha_{yyx}^i = -\alpha_{yyy}^i$.

The calculated band structure of MnBi_2Te_4 is plotted in Fig. 3(c), which shows an AFM semiconductor state. The local moment on Mn site is found to be $\sim 4.6 \mu_B$. These results are consistent with previous studies [33]. Using Eq. (4), the nonlinear response α_{yyy}^i is evaluated and plotted in Fig. 3(d) on the n -doping side. One observes that there is a peak $\sim 15 \mu_B \text{ V}^{-2} \text{ nm}^{-1}$ at about 52 meV above the conduction band minimum. This can be attributed to a small-gap region in the band structure, as indicated in Fig. 3(c), which hosts enhanced BCPs. At this doping level, under a moderate current density of $3 \times 10^7 \text{ A/cm}^2$ [14, 26], the generated staggered spin density can reach $1.4 \times 10^{-4} \mu_B/\text{nm}^3$. The resulting effective field B_T^i/α_G can be as large as ~ 11 T, which is more than one order of magnitude larger than the MAE (~ 0.2 meV per Mn [29, 33]) of MnBi_2Te_4 , suggesting the possibility of magnetic switching by nonlinear Néel torque.

The nonlinear character of Néel torque is manifested in a unique angular dependence. By rotating the driving current in the xy -plane, the generated spin density

exhibits the following angular dependence:

$$\delta \mathbf{s}^i = \alpha_{yyy}^i E^2 (\hat{x} \sin 2\phi + \hat{y} \cos 2\phi), \quad (9)$$

where ϕ is the angle between driving current and x axis. As shown in Fig. 4(a), the x and y components of the spin density have a simple $\sin 2\phi$ and $\cos 2\phi$ dependence, respectively. One sees that the sign of the nonlinear Néel torque is flipped when the driving direction is changed by $\pi/2$ (Fig. 4(b)), and it remains the same under the flip of driving current. This feature can be used to distinguish and extract the nonlinear response in experiment.

Application to even-layer insulating MnBi₂Te₄. The AFM ordering in MnBi₂Te₄ persists down to few layers [36, 43, 44]. Consider even-layer MnBi₂Te₄ in the AFM insulator state (i.e., without doping). Such systems break \mathcal{P} , however, \mathcal{PT} symmetry is preserved. According Table I, the intrinsic nonlinear Néel torque is the leading effect in this case.

Symmetry analysis shows that α_{yyy}^i is still the only independent response coefficient. Our calculation shows that for bilayer insulating MnBi₂Te₄, α_{yyy}^i can reach $\sim 0.4 \mu_B V^{-2} \text{nm}^{-1}$. In an insulator, E field can be applied through non-contact way and its magnitude can reach up to 10^8 V/m [14]. Under a moderate E field of 10^7 V/m, we estimate $B_T^i/\alpha_G \sim 3.2$ T (~ 0.8 meV), which is more than one order of magnitude larger than the reported MAE (~ 0.06 meV [44]) in bilayer MnBi₂Te₄. The result in four septuple-layer MnBi₂Te₄ is similar, with $B_T^i/\alpha_G \sim 1.7$ T.

Discussion. We have proposed the nonlinear Néel torque and revealed it as a new route to achieve electric control of centrosymmetric AFMs, where the existing paradigm of linear Néel torque fails. The strong Néel torques and the induced magnetic reorientation predicted in MnRh and MnBi₂Te₄ can be readily probed in experiment, e.g., by anisotropic magnetoresistance or Hall measurement, magneto-optical detection, and magnetic resonance measurement [26, 45–47].

Our findings greatly broaden the scope of Néel torque and AFM spintronics. Moreover, as noted, not just for \mathcal{P} -symmetric AFMs, the nonlinear mechanism may also dominate in certain \mathcal{P} -broken AFMs. It should also be mentioned that in systems where linear and nonlinear responses coexist, the nonlinear effect is not necessarily weaker, and it can in general be separated from the linear effect by symmetry, e.g., the linear torque is odd under the reversal of the driving field or current, whereas the nonlinear torque is even.

The formula and the calculation presented here are focused on the intrinsic contribution. In metallic systems, there also exist scattering induced extrinsic contributions. For example, we have evaluated the AFM nonlinear Edelstein effect, which results from the E -field induced second-order shift of Fermi surface. The corre-

sponding response tensor is given by

$$\alpha_{abc}^{\text{Edel},i} = -\frac{\tau^2}{2} \int [d\mathbf{k}] f'_0 (v_b \partial_{k_c} + v_c \partial_{k_b}) s_a^i, \quad (10)$$

where τ is the scattering time. Our calculation finds that for MnRh and doped MnBi₂Te₄, this extrinsic contribution is orders of magnitude smaller than the intrinsic one. Nevertheless, understanding extrinsic torques in AFMs is also an important task for future studies.

* These authors contributed equally to this work.

† liuhuiying@buaa.edu.cn

‡ congxiao@fudan.edu.cn

- [1] T. Jungwirth, X. Marti, P. Wadley, and J. Wunderlich, *Nature Nanotechnology* **11**, 231 (2016).
- [2] V. Baltz, A. Manchon, M. Tsoi, T. Moriyama, T. Ono, and Y. Tserkovnyak, *Rev. Mod. Phys.* **90**, 015005 (2018).
- [3] J. Han, R. Cheng, L. Liu, H. Ohno, and S. Fukami, *Nature Materials* **22**, 684 (2023).
- [4] A. Manchon, J. Železný, I. M. Miron, T. Jungwirth, J. Sinova, A. Thiaville, K. Garello, and P. Gambardella, *Rev. Mod. Phys.* **91**, 035004 (2019).
- [5] J. Železný, H. Gao, K. Výborný, J. Zemen, J. Mašek, A. Manchon, J. Wunderlich, J. Sinova, and T. Jungwirth, *Phys. Rev. Lett.* **113**, 157201 (2014).
- [6] J. Železný, H. Gao, A. Manchon, F. Freimuth, Y. Mokrousov, J. Zemen, J. Mašek, J. Sinova, and T. Jungwirth, *Phys. Rev. B* **95**, 014403 (2017).
- [7] J. Železný, P. Wadley, K. Olejník, A. Hoffmann, and H. Ohno, *Nature Physics* **14**, 220 (2018).
- [8] P. Wadley, B. Howells, J. Železný, C. Andrews, V. Hills, R. P. Campion, V. Novák, K. Olejník, F. Maccherozzi, S. S. Dhesi, S. Y. Martin, T. Wagner, J. Wunderlich, F. Freimuth, Y. Mokrousov, J. Kuneš, J. S. Chauhan, M. J. Grzybowski, A. W. Rushforth, K. W. Edmonds, B. L. Gallagher, and T. Jungwirth, *Science* **351**, 587 (2016).
- [9] M. J. Grzybowski, P. Wadley, K. W. Edmonds, R. Beardley, V. Hills, R. P. Campion, B. L. Gallagher, J. S. Chauhan, V. Novak, T. Jungwirth, F. Maccherozzi, and S. S. Dhesi, *Phys. Rev. Lett.* **118**, 057701 (2017).
- [10] J. Godinho, H. Reichlová, D. Kriegner, V. Novák, K. Olejník, Z. Kašpar, Z. Šobáň, P. Wadley, R. P. Campion, R. M. Otxoa, P. E. Roy, J. Železný, T. Jungwirth, and J. Wunderlich, *Nature Communications* **9**, 4686 (2018).
- [11] S. Y. Bodnar, L. Šmejkal, I. Turek, T. Jungwirth, O. Gomonay, J. Sinova, A. A. Sapozhnik, H.-J. Elmers, M. Kläui, and M. Jourdan, *Nature Communications* **9**, 348 (2018).
- [12] S. Reimers, Y. Lytvynenko, Y. Niu, E. Golias, B. Sarpi, L. Veiga, T. Denneulin, A. Kovacs, R. E. Dunin-Borkowski, J. Bläßer, *et al.*, *Nature Communications* **14**, 1861 (2023).
- [13] K. Olejník, V. Schuler, X. Marti, V. Novák, Z. Kašpar, P. Wadley, R. P. Campion, K. W. Edmonds, B. L. Gallagher, J. Garces, M. Baumgartner, P. Gambardella, and T. Jungwirth, *Nature Communications* **8**, 15434 (2017).
- [14] K. Olejník, T. Seifert, Z. Kašpar, V. Novák, P. Wadley,

- R. P. Campion, M. Baumgartner, P. Gambardella, P. Nèmec, J. Wunderlich, J. Sinova, P. Kužel, M. Müller, T. Kampfrath, and T. Jungwirth, *Science Advances* **4**, eaar3566 (2018).
- [15] See the Supplemental Material for the systematic symmetry constraints on nonlinear Néel spin-orbit torque, the detailed derivation of the intrinsic Néel torque theory, and the symmetry analysis and computational details of MnRh and MnBi₂Te₄.
- [16] Y. Gao, S. A. Yang, and Q. Niu, *Phys. Rev. Lett.* **112**, 166601 (2014).
- [17] Y. Gao, S. A. Yang, and Q. Niu, *Phys. Rev. B* **91**, 214405 (2015).
- [18] L. Dong, C. Xiao, B. Xiong, and Q. Niu, *Phys. Rev. Lett.* **124**, 066601 (2020).
- [19] C. Xiao, H. Liu, J. Zhao, S. A. Yang, and Q. Niu, *Phys. Rev. B* **103**, 045401 (2021).
- [20] C. Xiao, H. Liu, W. Wu, H. Wang, Q. Niu, and S. A. Yang, *Phys. Rev. Lett.* **129**, 086602 (2022).
- [21] H. Liu, J. Zhao, Y.-X. Huang, W. Wu, X.-L. Sheng, C. Xiao, and S. A. Yang, *Phys. Rev. Lett.* **127**, 277202 (2021).
- [22] K. Fukamichi, R. Umetsu, A. Sakuma, and C. Mitsumata, *chapter 4 Magnetic and Electrical Properties of Practical Antiferromagnetic Mn Alloys* (Elsevier, 2006).
- [23] L. Pál, E. Krén, G. Kádár, P. Szabó, and T. Tarnóczy, *Journal of Applied Physics* **39**, 538 (1968).
- [24] S. Khmelevskiy, A. B. Shick, and P. Mohn, *Phys. Rev. B* **83**, 224419 (2011).
- [25] I. J. Park, T. Lee, P. Das, B. Debnath, G. P. Carman, and R. K. Lake, *Applied Physics Letters* **114**, 142403 (2019).
- [26] L. Baldrati, C. Schmitt, O. Gomonay, R. Lebrun, R. Ramos, E. Saitoh, J. Sinova, and M. Kläui, *Phys. Rev. Lett.* **125**, 077201 (2020).
- [27] J. S. Kouvel, C. C. Hartelius, and L. M. Osika, *Journal of Applied Physics* **34**, 1095 (1963).
- [28] J. Tang and R. Cheng, *Phys. Rev. Lett.* **132**, 136701 (2024).
- [29] M. M. Otrokov, I. P. Rusinov, M. Blanco-Rey, M. Hoffmann, A. Y. Vyazovskaya, S. V. Ereemeev, A. Ernst, P. M. Echenique, A. Arnau, and E. V. Chulkov, *Phys. Rev. Lett.* **122**, 107202 (2019).
- [30] D. Zhang, M. Shi, T. Zhu, D. Xing, H. Zhang, and J. Wang, *Phys. Rev. Lett.* **122**, 206401 (2019).
- [31] Y. Gong, J. Guo, J. Li, K. Zhu, M. Liao, X. Liu, Q. Zhang, L. Gu, L. Tang, X. Feng, D. Zhang, W. Li, C. Song, L. Wang, P. Yu, X. Chen, Y. Wang, H. Yao, W. Duan, Y. Xu, S.-C. Zhang, X. Ma, Q.-K. Xue, and K. He, *Chinese Physics Letters* **36**, 076801 (2019).
- [32] J. Li, Y. Li, S. Du, Z. Wang, B.-L. Gu, S.-C. Zhang, K. He, W. Duan, and Y. Xu, *Science Advances* **5**, eaaw5685 (2019).
- [33] M. M. Otrokov, I. I. Klimovskikh, H. Bentmann, D. Estyunin, A. Zeugner, Z. S. Aliev, S. Gaß, A. U. B. Wolter, A. V. Koroleva, A. M. Shikin, M. Blanco-Rey, M. Hoffmann, I. P. Rusinov, A. Y. Vyazovskaya, S. V. Ereemeev, Y. M. Koroteev, V. M. Kuznetsov, F. Freyse, J. Sánchez-Barriga, I. R. Amiraslanov, M. B. Babanly, N. T. Mamedov, N. A. Abdullayev, V. N. Zverev, A. Alfonsov, V. Kataev, B. Büchner, E. F. Schwier, S. Kumar, A. Kimura, L. Petaccia, G. Di Santo, R. C. Vidal, S. Schatz, K. Kißner, M. Ünzelmann, C. H. Min, S. Moser, T. R. F. Peixoto, F. Reinert, A. Ernst, P. M. Echenique, A. Isaeva, and E. V. Chulkov, *Nature* **576**, 416 (2019).
- [34] Y. Deng, Y. Yu, M. Z. Shi, Z. Guo, Z. Xu, J. Wang, X. H. Chen, and Y. Zhang, *Science* **367**, 895 (2020).
- [35] C. Liu, Y. Wang, H. Li, Y. Wu, Y. Li, J. Li, K. He, Y. Xu, J. Zhang, and Y. Wang, *Nature Materials* **19**, 522 (2020).
- [36] S. Yang, X. Xu, Y. Zhu, R. Niu, C. Xu, Y. Peng, X. Cheng, X. Jia, Y. Huang, X. Xu, J. Lu, and Y. Ye, *Phys. Rev. X* **11**, 011003 (2021).
- [37] S. Li, T. Liu, C. Liu, Y. Wang, H.-Z. Lu, and X. C. Xie, *National Science Review* **11**, nwac296 (2023).
- [38] A. Gao, Y.-F. Liu, J.-X. Qiu, B. Ghosh, T. V. Trevisan, Y. Onishi, C. Hu, T. Qian, H.-J. Tien, S.-W. Chen, M. Huang, D. Bérubé, H. Li, C. Tzschaschel, T. Dinh, Z. Sun, S.-C. Ho, S.-W. Lien, B. Singh, K. Watanabe, T. Taniguchi, D. C. Bell, H. Lin, T.-R. Chang, C. R. Du, A. Bansil, L. Fu, N. Ni, P. P. Orth, Q. Ma, and S.-Y. Xu, *Science* **381**, 181 (2023).
- [39] N. Wang, D. Kaplan, Z. Zhang, T. Holder, N. Cao, A. Wang, X. Zhou, F. Zhou, Z. Jiang, C. Zhang, S. Ru, H. Cai, K. Watanabe, T. Taniguchi, B. Yan, and W. Gao, *Nature* **621**, 487 (2023).
- [40] H. Li, C. Zhang, C. Zhou, C. Ma, X. Lei, Z. Jin, H. He, B. Li, K. T. Law, and J. Wang, *Nature Communications* **15**, 7779 (2024).
- [41] Z. Lian, Y. Wang, Y. Wang, W.-H. Dong, Y. Feng, Z. Dong, M. Ma, S. Yang, L. Xu, Y. Li, B. Fu, Y. Li, W. Jiang, Y. Xu, C. Liu, J. Zhang, and Y. Wang, *Nature* **641**, 70 (2025).
- [42] J.-X. Qiu, B. Ghosh, J. Schütte-Engel, T. Qian, M. Smith, Y.-T. Yao, J. Ahn, Y.-F. Liu, A. Gao, C. Tzschaschel, H. Li, I. Petrides, D. Bérubé, T. Dinh, T. Huang, O. Liebman, E. M. Been, J. M. Blawat, K. Watanabe, T. Taniguchi, K. C. Fong, H. Lin, P. P. Orth, P. Narang, C. Felser, T.-R. Chang, R. McDonald, R. J. McQueeney, A. Bansil, I. Martin, N. Ni, Q. Ma, D. J. E. Marsh, A. Vishwanath, and S.-Y. Xu, *Nature* **641**, 62 (2025).
- [43] D. Ovchinnikov, X. Huang, Z. Lin, Z. Fei, J. Cai, T. Song, M. He, Q. Jiang, C. Wang, H. Li, Y. Wang, Y. Wu, D. Xiao, J.-H. Chu, J. Yan, C.-Z. Chang, Y.-T. Cui, and X. Xu, *Nano Letters* **21**, 2544 (2021).
- [44] D. Lujan, J. Choe, M. Rodriguez-Vega, Z. Ye, A. Leonardo, T. N. Nunley, L.-J. Chang, S.-F. Lee, J. Yan, G. A. Fiete, R. He, and X. Li, *Nature Communications* **13**, 2527 (2022).
- [45] V. Grigorev, M. Filianina, S. Y. Bodnar, S. Sobolev, N. Bhattacharjee, S. Bommanaboyena, Y. Lytvynenko, Y. Skourski, D. Fuchs, M. Kläui, M. Jourdan, and J. Demsar, *Phys. Rev. Appl.* **16**, 014037 (2021).
- [46] E. Cogulu, H. Zhang, N. N. Statuto, Y. Cheng, F. Yang, R. Cheng, and A. D. Kent, *Phys. Rev. Lett.* **128**, 247204 (2022).
- [47] P. Zhang, C.-T. Chou, H. Yun, B. C. McGoldrick, J. T. Hou, K. A. Mkhoyan, and L. Liu, *Phys. Rev. Lett.* **129**, 017203 (2022).